Combining Deep Eutectic Solvents with TEMPO-based Polymer Electrodes: Influence of Molar Ratio on Electrode Performance

Matthias Uhl,[a] Tanja Geng,[a] Philipp A. Schuster,[b] Benjamin W. Schick,[a] Matthias Kruck,[a] Alexander Fuoss,[a] Alexander J. C. Kuehne[b] and Timo Jacob*[a.c.d]

[a] M. Uhl, T. Geng, B. W. Schick, M. Kruck, A. Fuoss, Prof. Dr. T. Jacob
Institute of Electrochemistry
Ulm University
Albert-Einstein-Allee 47, 89081 Ulm, Germany
E-mail: timo.jacob@uni-ulm.de

[b] P. Schuster, Prof. Dr. A. J. C. Kuehne
Institute of Organic and Macromolecular Chemistry
Ulm University
Albert-Einstein-Allee 11, 89081, Ulm, Germany

[c] Prof. Dr. T. Jacob
Helmholtz-Institute Ulm (HIU) for Electrochemical Energy Storage
Helmholtzstr. 11, 89081 Ulm, Germany

[d] Prof. Dr. T. Jacob
Karlsruhe Institute of Technology (KIT)
P.O. Box 3640, 76021 Karlsruhe, Germany

Abstract: For sustainable storage of electrical energy, all-organic batteries based on redox-active polymers promise to become an alternative to conventional lithium ion batteries. Yet, polymers can only contribute to the goal of an all-organic cell as electrodes or as solid electrolytes. Here, we replace the electrolyte with a sustainable deep eutectic solvent (DES) composed of sodium bis(trifluoromethanesulfonyl)imide (NaTFSI) and *N*-methylacetamide (NMA), while using poly(2,2,6,6-tetramethylpiperidin-1-yl-oxyl methacrylate) (PTMA) as cathode. The successful combination of a DES with a polymer electrode is reported here for the first time. The electrochemical stability of PTMA electrodes in the DES at the eutectic molar ratio of 1:6 is comparable to conventional battery electrolytes. More viscous electrolytes with higher salt concentrations can hinder charging and discharging at high rates. Lower salt concentrations on the other hand lead to decreasing capacities and faster decomposition. The used eutectic mixture of 1:6 is best suited uniting high stability and moderate viscosity.

Introduction

The development of new organic batteries is driven by the need to address the climate crisis by strengthening non-fossil energy sources and compensating for net-fluctuations that renewable energy sources entail - since wind, sun, and tides are not synchronized with our demand for energy.[1–3] While full organic batteries are currently only foreseen as a niche technology[4], many organic polymers are already used in electrochemical storage systems, such as lithium ion batteries. Applications include polymer separators and binders, polymer electrolytes, and polymers as redox-active materials in battery electrodes.[5] A wide variety of classes of redox-active polymers are investigated, including organosulfur polymers, conjugated polymers, and organic radical polymers.[6]

One of these organic polymers is PTMA, with a polymethacrylate backbone and stable 2,2,6,6-tetramethylpiperidin-1-yl-oxyl (TEMPO) radicals in the periphery. More than 20 years ago, PTMA has been presented for the first time as a material for energy storage in rechargeable batteries. The fabricated batteries have demonstrated an average discharge voltage of 3.5 V and a discharge capacity of 77 $Ah \cdot kg^{-1}$ using Li as battery anode.[7,8] Further work improved the properties of PTMA electrodes by optimizing the carbon black and binder content in composite electrodes and by reducing the PTMA particle size by milling.[9] Customized changes in morphology can also be achieved by emulsion polymerization of PTMA. The resulting spherical particles, which can be controlled in size by the experimental conditions, exhibit a large surface area and are well applicable in composite electrodes.[10] Beside particles, PTMA brush polymers are of great interest today showing improvements especially in high-rate performance.[11] Since 2011, TEMPO radicals are also investigated for organic redox flow batteries.[12] Here, PTMA also works well as a redox-active compound in flow batteries, *e.g.* with a TEMPO derivative as redox mediator.[13]

For several applications including energy storage, *e.g.* in lithium ion batteries,[14–16] DESs are a rather new class of non-aqueous electrolytes. Originally introduced by Abbott and co-workers as catalysts for organic synthesis[17], DESs nowadays find wide application also in extraction and separation[18,19] and metal deposition.[20–22] If two components are mixed in their eutectic ratio, the binary mixture exhibits a freezing point depression. Depending on the composition, four different types of DESs can be distinguished. In contrast to all others, DESs type III do not contain metal ions but an organic salt, which is mixed with a hydrogen bond donor. When replacing the organic salt with a metal salt, the DES is termed type IV. Both types III and IV are highly variable in their composition and therefore very versatile in their physical and electrochemical behavior. Especially DESs type III are typically considered as green alternatives to solvents and ionic liquids, since most of the commonly used components are non-toxic and environmentally-friendly.[20,23]

Both concepts, organic polymer electrodes and deep eutectic solvents, aim for environmentally-friendly and sustainable future energy storage. However, DESs as electrolytes have not yet been combined with organic redox-active polymers, obviating understanding and transfer of these systems into application. In the present study, we show that DESs can indeed serve as suitable electrolytes for all-organic batteries with redox-active polymer electrodes. We go beyond the proof-of-concept by investigating the influence of the molar composition of the DES in detail, finding a high influence on the electrochemical stability, activity, and high-rate performance of the redox-active polymer. Among several mixtures, the eutectic mixture of the used DES is highlighted.

Since PTMA is well investigated in several electrolytes showing high stability and activity, it is used as active material for the polymer electrodes. The utilized DES consists of NaTFSI and NMA, which have been selected because of their high electrochemical stability in the potential region of interest. Physical characterization of the DES is performed by differential scanning calorimetry (DSC) to determine the eutectic composition and by determination of the viscosity and density of the different mixtures. The electrochemical performance of the PTMA electrodes in contact with the DES is evaluated by cyclic voltammetry (CV) and galvanostatic charge–discharge cycling in half cells.

Results and Discussion

Thermal characterization of the DES

To determine the eutectic composition of mixtures consisting of NaTFSI and NMA, DSC measurements of various mixtures in different molar ratios are performed. The heating curve of each sample has been recorded from -180 to 80 °C with a heating rate of 1 °C·min^{-1}, as shown in Figure 1A in the relevant temperature range. Below -50 °C, the curves exhibit a step in the baseline corresponding to the glass transition. Since the samples have been cooled fast before the depicted heating step, recrystallization occurs upon heating causing exothermic peaks. If the temperature is increased further, the samples melt and endothermic peaks are observable. The relatively slow heating rate is chosen to achieve a better separation of the recrystallization and melting events, so that the melting enthalpies can be reliably determined, while still being able to analyze the glass transitions.

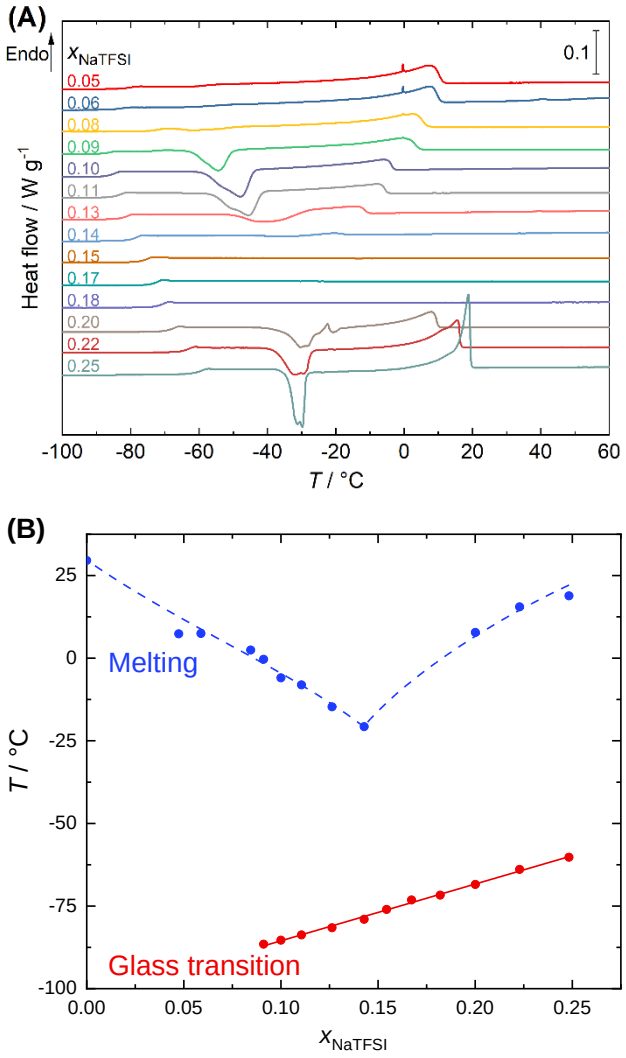

Figure 1. (A) DSC curves of NaTFSI:NMA mixtures in various compositions recorded with a heating rate of 1 °C·min^{-1}. The endothermic heat flow is shown as a function of temperature in the relevant range and for better readability, the thermograms are shifted against each other. (B) Phase diagram of the NaTFSI:NMA DES as a function of the mole fraction of NaTFSI. The glass transition temperatures (red) are fitted with a linear fit. The temperatures of the melting peak (blue) are approximated by the dashed line as guide for the eye.

The glass transition temperature of each curve is determined by the temperature of a tangent to the step itself at half height of the step. Thereby, the enthalpic recovery, visible as a small endothermic peak at the end of the glass transition, is not considered. The glass transition temperature increases linearly with increasing amount of NaTFSI for molar ratios of $x_{NaTFSI} \geq 0.09$, as shown in Figure 1B in red.

To determine the eutectic ratio of the NaTFSI:NMA DES, the melting peaks are analyzed. Normally, one would expect two melting peaks for each sample with one occurring at the same temperature independently of the composition. This peak would correspond to the melting of the eutectic and therefore, one could obtain the solidus curve of the phase diagram and from that, the eutectic temperature. For example, this is the case for various DESs type III, whose eutectic temperature has been determined accordingly.[21,24] However, similar behavior is not observed for the NaTFSI:NMA mixtures (Figure 1A). We assume that this mixture does not crystallize and

subsequently cannot melt. Instead, it is forming a glass and therefore, only the glass transition is observable. The second melting event is expected to take place at a higher temperature depending on the composition and corresponding to melting of the excess component, thus yielding the liquidus curve. As only one melting event occurs at variable temperatures for the NaTFSI:NMA DES, we assume that it corresponds to melting of the respective excess component. The melting temperatures leading to the liquidus curve are determined as the peak temperatures because at the peak, the excess component in each sample has molten completely and the whole mixture will be liquid. Therefore, the melting peak temperatures of the different samples are given in Figure 1B in blue as a function of composition.

The melting temperature first decreases with increasing amount of NaTFSI until $x_{NaTFSI} = 0.14$. The mixtures with $0.15 \leq x_{NaTFSI} \leq 0.18$ exhibit no processes other than the glass transition, but for $x_{NaTFSI} \geq 0.2$ the melting temperatures increase with NaTFSI content. This leads to a minimum at $x_{NaTFSI} = 0.14$, which is a good estimate for the eutectic composition and corresponds to a NaTFSI:NMA ratio of about 1:6. Further evidence for this ratio can be found in a plot of the melting enthalpies as a function of the molar ratio (Figure S1). If the melting peak corresponds to melting of the excess component, it should exhibit a higher enthalpy, the more the ratio deviates from the eutectic ratio. Therefore, we expect a minimum at the eutectic ratio, which is at $x_{NaTFSI} = 0.15$ (NaTFSI:NMA 1:5.8), a ratio very similar to the one determined from the DSC curves themselves.

NaTFSI:NMA mixtures without recrystallization and melting have also been observed previously in DSC experiments with a heating rate of 10 °C·min^{-1}.[25] The same is true for mixtures of LiTFSI with different sulfonamide-based hydrogen bond donors.[26] In a LiTFSI:NMA DES, a glass transition and a melting peak dependent on the molar ratio have been observed by DSC measurements.[15,27] For a LiTFSI molar ratio between 0.15 and 0.2, only a glass transition occurs, which is analogous to our observations using NaTFSI. In the case of LiTFSI, a eutectic ratio of $x_{LiTFSI} = 0.2$ and a eutectic temperature of -72 °C have been reported, whereby the latter corresponds to the glass transition temperature of the eutectic mixture.[15] For this DES, a eutectic ratio of $x_{LiTFSI} = 0.17$ has been calculated theoretically.[14]

As there are several ratios with LiTFSI as well as NaTFSI without melting peak, the eutectic ratio can only be estimated, as described before. Since one cannot be entirely sure about the exact course of the liquidus curve and since the solidus curve is not observed, no conclusion is drawn about the eutectic temperature of the NaTFSI:NMA DES. However, with a large freezing-point depression of the eutectic mixture ($x_{NaTFSI} = 0.14$, NaTFSI:NMA 1:6) of more than 50 °C with respect to the melting point of pure NMA, NaTFSI:NMA is clearly a DES. For the mixtures with $x_{NaTFSI} \leq 0.06$, a small endothermic peak appears around 0 °C (Figure 1A), which is also observable in pure

NMA (Figure S2) and has been detected previously.[25] It is probably connected to the residual water content of undried NMA.

Electrochemical characterization

In the next step, we investigated the applicability of DESs as electrolytes in all-organic batteries. The DES NaTFSI:NMA is combined with well-investigated polymer electrodes based on PTMA as redox-active material.[10] The fabrication of the electrodes is described in the experimental section. The influence of the molar composition of the DES on the electrochemical behavior of PTMA electrodes is analyzed using the before-mentioned DES in several molar ratios. The quality and performance of the self-made electrodes are comparable to those of Muench and co-workers[10] since the electrochemical behaviour and the specific capacity of the electrodes in 1 M 1-butyl-1-methylpyrrolidinium bis(trifluormethylsulfonyl)imid ($Pyr_{14}TFSI$) in propylene carbonate are almost identical (Figures S3 and S4). The oxidation of the TEMPO radical units and the reduction in the reverse scan direction is taking place at approximately 600 mV *vs.* Ag pseudo reference electrode. The maximum specific discharge capacity is roughly 94 $mAh \cdot g^{-1}$.

Using the DES NaTFSI:NMA instead of the propylene carbonate-based electrolyte for cyclic voltammetry in half-cells with PTMA electrodes (Figure 2), the oxidation and reduction of the TEMPO units is also observed at potentials around 600 mV *vs.* Ag. Small deviations in the redox potential are caused by minor instabilities of the pseudo reference electrode. The peaks in the cyclic voltammograms of the PTMA electrode in the DESs exhibit smaller peak currents but a slower current decay after reaching the maximum current than in the case of the carbonate-based electrolyte (Figure S3). Positive of 1 V *vs.* Ag, irreversible oxidation occurs, most likely caused by anodic decomposition of the electrolyte. This is more pronounced for DESs with lower amounts of NaTFSI (Figure 2C). According to De Sloovere and co-workers, the reason for the higher electrochemical stability in more concentrated DESs is the strong interaction between the ions and the solvent in the NaTFSI:NMA mixture leading to a decreasing energy of the highest occupied molecular orbital (HOMO) of NMA with increasing salt concentration.[25] The resulting decomposition potentials for highly concentrated electrolytes correspond well to the values we found in our study. The stabilizing effect of a high share of NaTFSI will be discussed further below in more detail.

Additionally, there is a significant difference in the initial activity between electrolytes with salt concentrations higher than or equal to the eutectic mixture (Figures 2A and B) and those with lower salt contents (Figures 2C and S5). For high salt concentrations, peak currents are increasing within the first cycles after assembling and equilibrating the electrochemical cell for 5 hours. This behaviour is more pronounced in the 1:4 mixture than in the eutectic mixture of 1:6. Lower concentrated electrolytes cause high currents right from the beginning, which are in some

cases accompanied with a quite large irreversible oxidation in the initial cycle (Figure S5). In contrast to the DESs with high salt concentration, especially cathodic currents are rather decreasing during cycling.

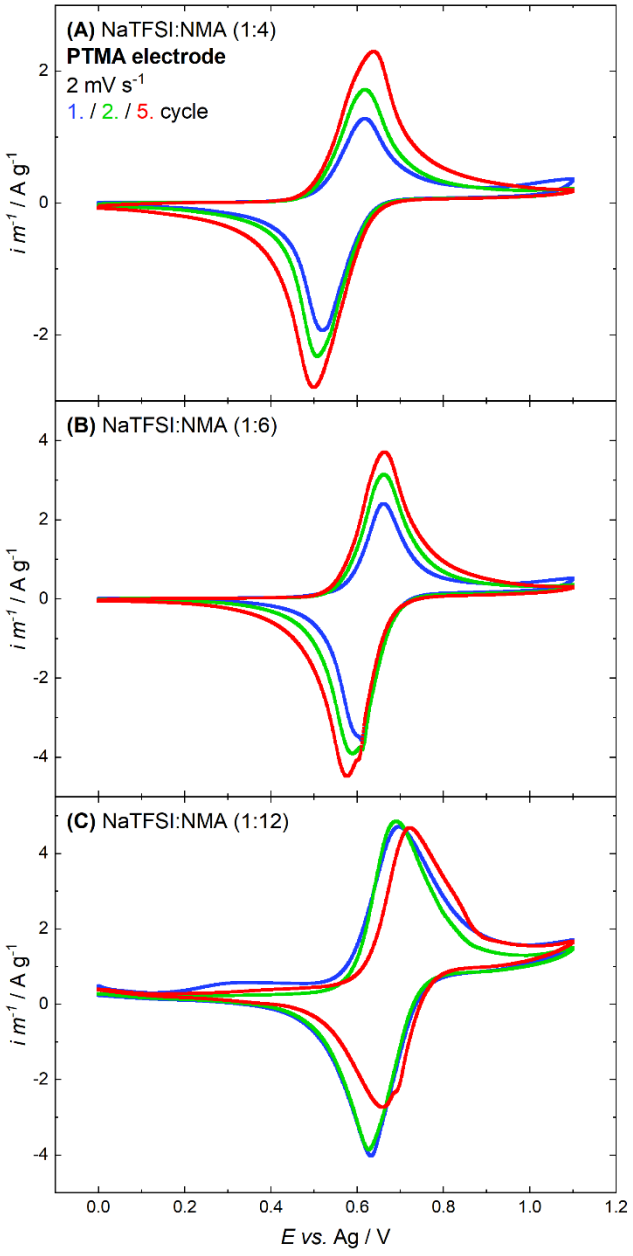

Figure 2. Cyclic voltammograms of PTMA electrodes in NaTFSI:NMA DESs with a molar ratio of (A) 1:4, (B) 1:6, and (C) 1:12 showing the 1st (blue), 2nd (green), and 5th (red) cycle at a scan rate of 2 mV·s^{-1}.

To unravel the origin of the differences in the cyclic voltammograms (Figure 2), viscosity and density of various mixtures were measured at different temperatures. In Figure 3, the dynamic viscosity η at 20, 25, 40, and 80 °C is shown as a function of the molar ratio of NaTFSI. It is evident that the higher the salt content, the higher is the viscosity, and there is no exception for the eutectic 1:6 mixture (x_{NaTFSI} = 0.14). Moreover, lower temperatures entail

higher viscosities. Further evaluation of the viscosity and density is given in the Supporting Information (Figures S6 and S7).

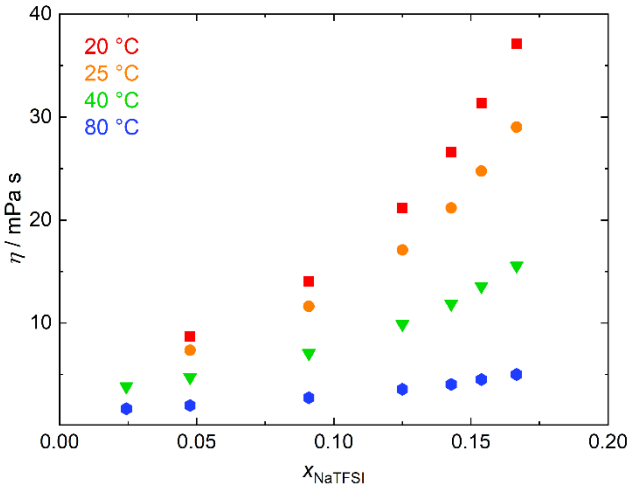

Figure 3. Dynamic viscosity at 20 (red), 25 (orange), 40 (green), and 80 °C (blue) for NaTFSI:NMA mixtures in different molar ratios.

Referring to the high viscosity of DESs at room temperature at the eutectic composition and with higher salt concentration, the initial increase in capacity during cycling could be caused by a disadvantageous wetting behaviour compared to less viscous electrolytes. The time to wet and infiltrate the internal surface of smaller pores of the electrode with electrolyte may be longer especially since the unpolar polymer chains interact stronger with neutral NMA molecules than with the dissolved salt. This leads to disabled electrolyte contact for parts of the active material and with this to initially lower capacities.[28,29]

After these initial cycles, voltammograms are recorded at a higher scan rate to monitor the cycling stability (Figure 4). Here, the advantage of highly-concentrated electrolytes is clearly observable. With mixtures in the molar ratio 1:4 and 1:6 (Figures 4A and B), PTMA exhibits excellent cycling stability for 100 cycles. The peak shape and peak current densities remain almost unchanged over the whole period. In this case, the investigated DESs perform equally good as the electrolyte based on propylene carbonate (Figure S8).

For lower salt concentrations (Figures 4C and S9), the cycling stability changes dramatically. Already during the first cycles, the currents caused by the oxidation of the TEMPO radical decrease continuosly, whereas the decomposition currents at the positive end of the potential stability window remain unaffected, indicating continuous degradation.

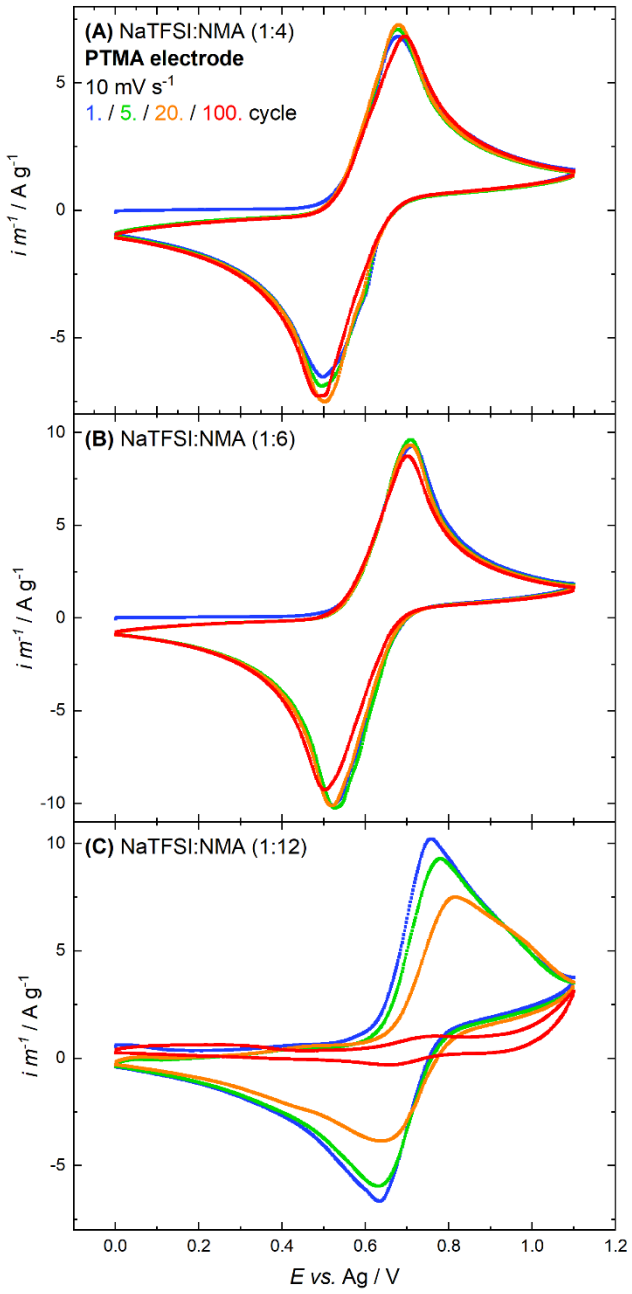

Figure 4. Cyclic voltammograms of PTMA electrodes in NaTFSI:NMA DESs with a molar ratio of (A) 1:4, (B) 1:6, and (C) 1:12 at a scan rate of 10 mV·s^{-1} to test the cycling stability. The 1st (blue), 5th (green), 20th (orange), and 100th (red) cycle are shown.

The reason for the high electrochemical stability of the DES in its eutectic ratio and at higher salt concentrations is explained by the effect of stabilization of the NMA molecules by the salt. A high concentration of ions in the electrolyte leads to complexed supramolecular network-like 3D-structures in the liquid. Through hydrogen bonding and other interactions, reactive groups of the molecules are stabilized and therefore protected from decomposition reactions. This is also reflected in a decrease in energy of the HOMO of the solvent.[30,31] For DESs, this is equally valid. Hammond and co-workers found such complexed network-like layered structures in a DES composed of choline chloride and urea in its eutectic composition.[32] In this binary mixture, all neutral molecules interact with the

ions in the DES. For the DES NaTFSI:NMA used in this study, De Sloovere and co-workers also found a stabilizing effect by high salt concentrations experimentally, as well as by calculating the HOMO energies with density functional theory. Because of the decrease in HOMO energy, the oxidation of NMA shifts to higher potentials.[25] In DESs with lower salt concentrations than the eutectic ratio, non-complexed or not fully complexed NMA molecules are less stable causing continuous electrolyte decomposition at potentials higher than 1 V.

Nevertheless, a specific reason for the capacity fading in lower-concentrated DESs cannot be given for granted. Possibly, the excess solvent slowly dissolves PTMA, thus reducing the amount of redox-active material on the electrode. At least this is known to happen for structurally similar radical-polymers in carbonate solvents.[33] However, in case of PTMA in a highly-concentrated DES and in a propylene carbonate electrolyte, the capacities in cyclic voltammetry and the macroscopic appearance of the electrodes remain unchanged. An alternative explanation is that decomposition products of the non-complexed NMA molecules could block active sites on the PTMA electrodes either by reacting with the radical or the cationic group of the PTMA itself or by covering the electrode surface with an insoluble non-conductive organic film. The blocking of pores by decomposition products of organic electrolytes is reported *e.g.* by Azaïs and co-workers.[34]

Galvanostatic cycling

To get an insight into the behavior of PTMA as active material in battery cathodes, galvanostatic charge–discharge measurements with a rate of 10 C were performed using the same electrochemical setup as for cyclic voltammetry. Since PTMA is commonly used as a cathode material for batteries[11,35,36], the oxidation of the TEMPO radicals is defined as the charging step and the accompanying reduction corresponds to discharging. To calculate the Coulombic efficiency *CE*, the specific discharge capacity $C_{sp,dc}$ is divided by the specific charge capacity $C_{sp,c}$ of the same cycle n (Equation 1).

$$CE = \frac{C_{\mathrm{sp,dc}}(n)}{C_{\mathrm{sp,c}}(n)} \quad (1)$$

The capacity retention *CR* is defined by the specific discharge capacities of two following cycles (Equation 2).[37]

$$CR = \frac{C_{\mathrm{sp,dc}}(n+1)}{C_{\mathrm{sp,dc}}(n)} \quad (2)$$

As discussed before, the salt concentration in the DES has a significant influence on the initial capacity as well as long-term electrochemical stability and activity. This is also true for the galvanostatic measurements (Figure 5). For

the DES in its eutectic ratio of 1:6, the specific capacity increases in the first charging steps just as observed by cyclic voltammetry (Figure 2B), leading to a capacity retention higher than 1 in the beginning. After reaching a limit of roughly 70 mAh·g^{-1} after 10 cycles, the Coulombic efficiency stabilizes at around 97%. It is accompanied by a capacity retention of more than 99% leading to a slowly decreasing specific capacity. Compared to the electrochemical long-term stability in cyclic voltammetry, PTMA exhibits a little higher capacity loss in galvanostatic measurements. After 100 cycles, the capacity reaches approximately 70% of the maximum value. One factor for this more prominent capacity fading is the measurement time. Hundred galvanostatic charge–discharge cycles with a rate of 10 C last up to 20 hours and take therefore roughly three times longer than 100 cycles in CV at 10 mV·s^{-1}. If dissolution of neutral or charged PTMA is meant to be the reason for decreasing capacities, this effect of time is rather relevant.

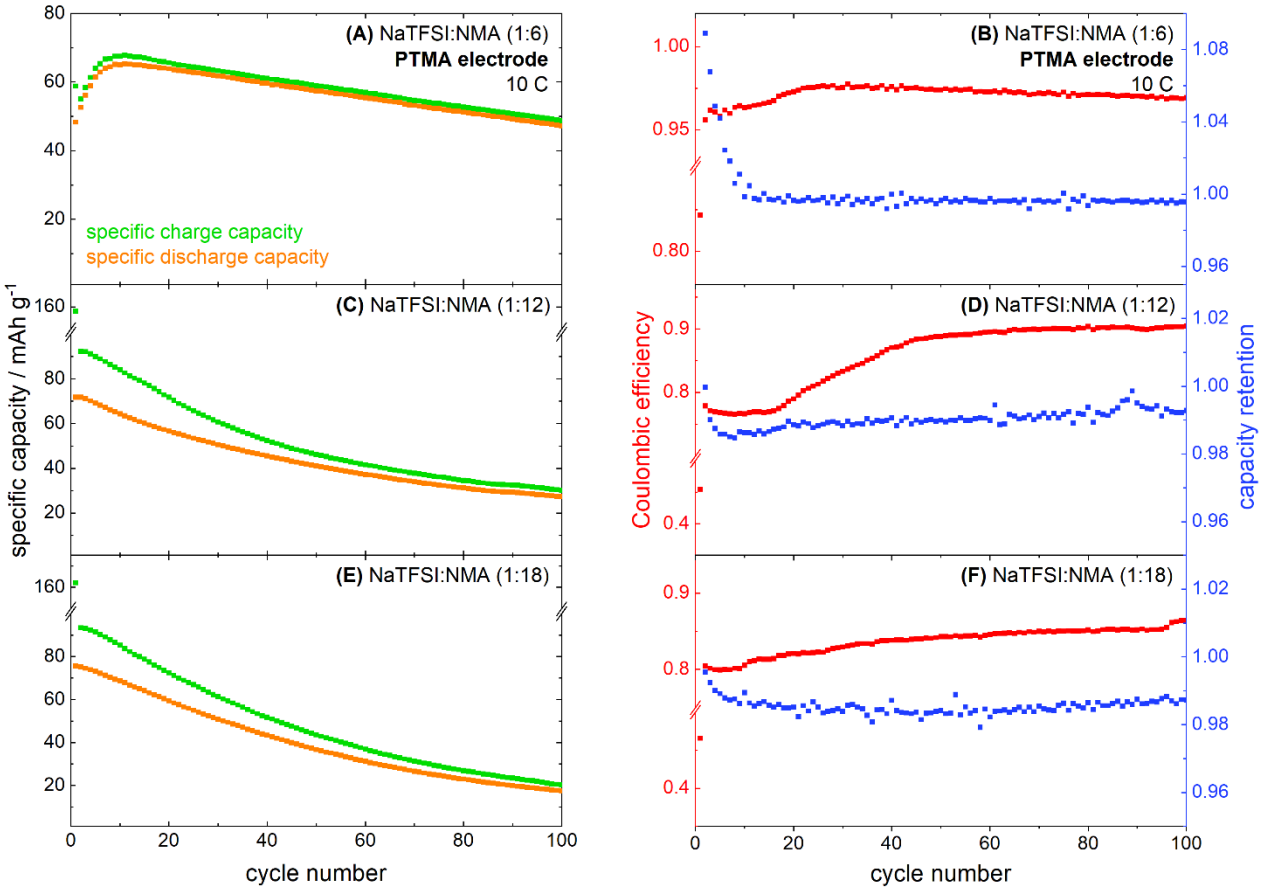

Figure 5. Chronopotentiometric charge–discharge cycling of PTMA electrodes in NaTFSI:NMA DESs with a molar ratio of (A, B) 1:6, (C, D) 1:12, and (E, F) 1:18 between 0 V and 1 V *vs.* Ag at a rate of 10 C (A, C, E). Specific charge (green) and discharge (orange) capacities for 100 cycles; (B, D, F) corresponding Coulombic efficiency (red) and capacity retention (blue).

For the DESs with lower salt concentration, the electrochemical behavior during charge-discharge cycling is comparable to the previous findings with cyclic voltammetry (Figures 4C and S9). Already in the initial cycle, the maximum specific discharge capacity is achieved followed by a faster decrease in capacity than for the eutectic

mixture. The Coulombic efficiency is lower than 90% indicating an irreversible oxidation process which is also observed in the cyclic voltammograms (Figures 4C and S9). The capacity retention of 98–99% reflects the continuous decrease in capacity. High irreversible currents are observed for the initial charging step, as seen by cyclic voltammetry (Figure S5). This phenomenon can be associated with electrolyte decomposition.[38]

Because of the high rates for charging and discharging, the maximum specific discharge capacity of the PTMA electrodes is around 70 $mAh \cdot g^{-1}$ for all tested DESs. For a lower rate of 1.5 C in the DES at the eutectic mixture (Figure S10A), the maximum specific discharge capacity is roughly 30% higher. This is in agreement with half-cell tests of PTMA electrodes of Muench and co-workers in a carbonate-based electrolyte[10], which is able to achieve efficient and stable cycling of PTMA electrodes even at 10 C (Figure S4).

Surprisingly, it is not possible to achieve efficient galvanostatic charging and discharging with NaTFSI:NMA 1:4 at a rate of 10 C. At such high currents, the measured capacities are far below the expected values. The potential profiles do not show a clear potential plateau at the expected value of 0.6 V. Therefore, this electrolyte is unsuited for charging and discharging at high rates. The reason for this seems to be the high viscosity. Beside the disadvantageous wetting of the electrodes[28,29], high salt concentrations can hinder salt dissociation and lower the ionic conductivity of the electrolyte.[25]

At 1.5 C and after a dwell time of 70 h, NaTFSI:NMA 1:4 exhibits an improved performance. The Coulombic efficiency is relatively high (97.5%), accompanied by a capacity retention close to 1 (Figures S10A and B). The maximum specific discharge capacity reaches an overall limit of 90 $mAh \cdot g^{-1}$, which is close to the capacity determined in the propylene carbonate-based electrolyte (Figure S4). Within 100 cycles, the capacity decreases by more than 50% in total for the highly-concentrated DES.

With the eutectic mixture NaTFSI:NMA 1:6, the electrochemical activity of PTMA decreases faster than for more concentrated DES (Figures S10C and D). This is most likely attributed to the higher share of NMA as discussed before. It is noteworthy to mention, that after the long dwell time of 70 h, the maximum discharge capacity of 87 $mAh \cdot g^{-1}$ is achieved directly in the first cycle and no further activation is needed. This also indicates that PTMA is not dissolved or passivated before the first oxidation. More likely, the cationic TEMPO-moieties dissolve or react, thereby leading to decreasing capacities during cycling which is more relevant when using low cycling rates.

Conclusion

In this study, we proved the successful combination of DESs with polymer electrodes paving the way to a new type of sustainable all-organic batteries. In this regard, the application of the DES NaTFSI:NMA as an electrolyte for

redox-active PTMA electrodes has been investigated. The electrochemical performance of the half-cells highly depends on the molar composition of the electrolyte. The eutectic ratio was determined by DSC to be approximately 1:6. In this mixture, a good compromise between high electrochemical cycling stability, especially during the CV measurements, and moderate viscosity is achieved. Coulombic efficiencies of 97% are achieved in galvanostatic charge–discharge cycling of the PTMA half-cells at a rate of 10 C. The electrochemical stability is even better when using cyclic voltammetry reflecting the compatibility of the DES with PTMA electrodes. DESs with lower salt concentrations than the eutectic mixture show higher decomposition currents at the positive end of the potential stability window due to higher HOMO energies for NMA. Also, they lead to a faster decrease in electrode capacity indicating instabilities due to unbound solvent molecules. Either PTMA is slowly dissolving in the excess NMA, or the decomposition products block the active sites of the polymer electrode.

Highly-concentrated DESs exhibit higher electrochemical stability but also higher viscosity, thereby leading to an increase in capacity during the first few cycles. This is most probably due to disadvantageous wetting behavior. Since the conductivity of the DES decreases at concentrations higher than the eutectic ratio, fast charging and discharging is partially prevented.

With this work, the applicability of DESs for future energy storage in all-organic batteries as sustainable alternative has been proven successfully. The importance and advantage of using the DES in its eutectic ratio has been discussed in detail. In terms of environmental friendliness, the use of DESs type III would even be more advantageous than the here investigated DES type IV. However, current DESs type III exhibit poor anodic stability at the oxidation potential of PTMA. For future studies, the combination of DESs and redox-active polymers need to be chosen carefully to match the electrochemical stability window of the electrolyte with the redox potential of the polymer. Additionally, other factors such as viscosity of the electrolyte and solubility of the active material in the electrolyte are crucial parameters for a well-performing organic battery.

Experimental Section

Fabrication of electrolytes

N-methylacetamide (Aldrich chemicals, 99%) was purified by distillation. NaTFSI (Solvionic, 99.9%), 1-butyl-1-methylpyrrolidinium bis(trifluormethylsulfonyl)imid (Merck, >99%), and propylene carbonate (Alfa Aesar, 99%) were used as received. The electrolytes were mixed at room temperature under N2 atmosphere (H2O < 0.5 ppm, O2 < 0.5 ppm) in a glovebox (M. Braun). For the electrochemical measurements, molecular sieve (3 Å, Merck) was added to all electrolytes to reduce the water content to less than 10 ppm. This was checked by Karl-Fischer-

Titration (KF-Coulmeter 851 by Metrohm, with Hydranal Coulmat AG electrolyte by Honeywell). The molecular sieve was boiled in ultrapure water and afterwards dried for 5 h at 350 °C under N_2 atmosphere prior to use.

Physical characterization of electrolytes

The DSC measurements were conducted in a DSC 250 (TA Instruments) with a liquid nitrogen cooling system. Calibration of the device was carried out with indium so that the deviation of temperature was below 0.2 °C and deviation of enthalpy less than 1%. Tzero aluminum pans (TA Instruments) were filled in the glovebox and closed with a normal and a hermetic lid to prevent ingress of oxygen and water. During the measurements, the DSC cell was purged with helium 5.0 (25 mL·min^{-1}). First, the samples were heated to 80 °C to ensure that they are all liquid, then cooled with 10 °C·min^{-1} to -180 °C and heated with 1 °C·min^{-1} to 80 °C. Between each step, the temperature was held isothermally for 5 min. Since only the heating step with glass transition, recrystallization, and melting is of interest, only this step is presented. The data was recorded and evaluated with the TRIOS software (TA Instruments).

Viscosity and density measurements were performed using a SVM 3001 viscometer (Anton Paar). The samples, which were liquid at room temperature, were filled into a syringe in the glovebox and transferred directly into the viscometer to minimize contact with air. Density and dynamic viscosity of each sample were measured at 20, 25, 30, 40, 50, 60, 70, and 80 °C. The reproducibility of the temperature is 0.03 °C, that of the viscosity is 0.35%, and that of the density is 0.0001 g·cm^{-3}.

Fabrication of electrodes

PTMA particles (size 100 nm, degree of oxidation 77% ± 12%) received from FSU Jena[10], SuperP® carbon black (Alfa Aesar) and carboxymethyl cellulose sodium salt (Sigma Aldrich) (mass ratio 35:60:5) were dispersed in water (0.055 µS cm^{-1}) using a laboratory dispersing instrument (Ultra-Turrax T8® by IKA). The obtained slurry was allowed to stand for at least 30 minutes and afterwards mixed again at full strength for 10 minutes. Before the slurry was doctor-bladed on aluminum foil (Korff, thickness 15 µm), the foil was pretreated with aqueous KOH solution (pH 12) for 1 minute and dried. The film was allowed to dry slowly at room temperature (about 12 h). For the electrochemical measurements, round electrodes with a diameter of 12 mm were punched out of the film.

Electrochemical setup and measurements

All electrochemical measurements were performed in a Swagelok-type T-shaped 3-electrode cell setup. Graphite (Goodfellow, 99.997%) was used as counter electrode and a thermally annealed Ag-wire (MaTecK, 99.99%) served as reference electrode. The geometric area of the working and counter electrode is 1.13 cm^2. One glass fiber separator (Whatman GF/B) soaked with 60 µL of electrolyte was positioned each in between the working and the reference electrode and the reference and the counter electrode respectively. The cells were assembled in the above-mentioned glovebox under N_2 atmosphere. The measurements were performed with an Interface 1010B potentiostat (Gamry Instruments). If not mentioned differently, the cells were hold at open circuit potential for one hour to equilibrate. Cyclic voltammetry was first done at 2 mV s^{-1} and afterwards at 10 mV·s^{-1} in the same cell. Galvanostatic charge-discharge cycling was performed using the same preparation procedure.

Acknowledgements

We thank Dr. Simon Muench and Prof. Dr. Ulrich Schubert for providing PTMA particles for the investigated polymer electrodes.

This work contributes to the research performed at CELEST (Center for Electrochemical Energy Storage Ulm-Karlsruhe) and we thank the German Research Foundation (DFG) for funding under Project ID 390874152 (POLiS Cluster of Excellence), and for funding within the priority program SPP 2248 Polymer-based Batteries (Project ID 441209207).

Keywords: deep eutectic solvent • PTMA electrode • organic battery • sustainable chemistry • electrochemistry

CRediT

M. Uhl: Conceptualization, Formal Analysis, Investigation, Validation**,** Visualization, Writing – Original Draft Preparation

T. Geng: Conceptualization, Formal Analysis, Investigation, Validation, Visualization, Writing – Original Draft Preparation

P. A. Schuster: Investigation, Writing – Original Draft Preparation

B. W. Schick: Conceptualization, Writing – Review & Editing

M. Kruck: Investigation, Writing – Review & Editing

A. Fuoss: Investigation

A. J. C. Kuehne: Funding Acquisition, Resources, Supervision, Writing – Review & Editing

T. Jacob: Funding Acquisition, Resources, Supervision, Writing – Review & Editing

References

[1] D. Larcher, J.-M. Tarascon, *Nat. Chem.* **2015**, *7*, 19–29.

[2] J. Kim, J. H. Kim, K. Ariga, *Joule* **2017**, *1*, 739–768.

[3] N. Goujon, N. Casado, N. Patil, R. Marcilla, D. Mecerreyes, *Prog. Polym. Sci.* **2021**, *122*, 101449.

[4] J. P. Esquivel, P. Alday, O. A. Ibrahim, B. Fernández, E. Kjeang, N. Sabaté, *Adv. Energy Mater.* **2017**, *7*, DOI 10.1002/aenm.201700275.

[5] D. Mecerreyes, L. Porcarelli, N. Casado, *Macromol. Chem. Phys.* **2020**, *221*, 1900490.

[6] S. Muench, A. Wild, C. Friebe, B. Häupler, T. Janoschka, U. S. Schubert, *Chem. Rev.* **2016**, *116*, 9438–9484.

[7] K. Nakahara, S. Iwasa, M. Satoh, Y. Morioka, J. Iriyama, M. Suguro, E. Hasegawa, *Chem. Phys. Lett.* **2002**, *359*, 351–354.

[8] H. Nishide, S. Iwasa, Y. J. Pu, T. Suga, K. Nakahara, M. Satoh, *Electrochim. Acta* **2004**, *50*, 827–831.

[9] S. Komaba, T. Tanaka, T. Ozeki, T. Taki, H. Watanabe, H. Tachikawa, *J. Power Sources* **2010**, *195*, 6212–6217.

[10] S. Muench, P. Gerlach, R. Burges, M. Strumpf, S. Hoeppener, A. Wild, A. Lex-Balducci, A. Balducci, J. C. Brendel, U. S. Schubert, *ChemSusChem* **2021**, *14*, 449–455.

[11] R. Rohan, M.-K. Hung, Y.-F. Yang, C.-W. Hsu, C.-K. Yeh, Y.-L. Chang, J.-T. Lee, *ACS Appl. Polym. Mater.* **2022**, *4*, 2365–2372.

[12] Z. Li, S. Li, S. Liu, K. Huang, D. Fang, F. Wang, S. Peng, *Electrochem. Solid-State Lett.* **2011**, *14*, 171–174.

[13] E. Schröter, C. Stolze, A. Saal, K. Schreyer, M. D. Hager, U. S. Schubert, *ACS Appl. Mater. Interfaces* **2022**, *14*, 6638–6648.

[14] W. Zaidi, A. Boisset, J. Jacquemin, L. Timperman, M. Anouti, *J. Phys. Chem. C* **2014**, *118*, 4033–4042.

[15] A. Boisset, S. Menne, J. Jacquemin, A. Balducci, M. Anouti, *Phys. Chem. Chem. Phys.* **2013**, *15*, 20054–20063.

[16] J. Wu, Q. Liang, X. Yu, Q. Lü, L. Ma, X. Qin, G. Chen, B. Li, *Adv. Funct. Mater.* **2021**, *31*, 2011102.

[17] A. P. Abbott, G. Capper, D. L. Davies, H. L. Munro, R. K. Rasheed, V. Tambyrajah, *Chem. Commun.* **2001**, 2010–2011.

[18] X. Li, K. H. Row, *J. Sep. Sci.* **2016**, *39*, 3505–3520.

[19] M. Ruesgas-Ramón, M. C. Figueroa-Espinoza, E. Durand, *J. Agric. Food Chem.* **2017**, *65*, 3591–3601.

[20] E. L. Smith, A. P. Abbott, K. S. Ryder, *Chem. Rev.* **2014**, *114*, 11060–11082.

[21] T. Geng, S. J. Zeller, L. A. Kibler, M. U. Ceblin, T. Jacob, *ChemElectroChem* **2022**, *9*, DOI 10.1002/celc.202101283.

[22] M. U. Ceblin, S. Zeller, B. Schick, L. A. Kibler, T. Jacob, *ChemElectroChem* **2019**, *6*, 141–146.

[23] B. B. Hansen, S. Spittle, B. Chen, D. Poe, Y. Zhang, J. M. Klein, A. Horton, L. Adhikari, T. Zelovich, B. W. Doherty, B. Gurkan, E. J. Maginn, A. Ragauskas, M. Dadmun, T. A. Zawodzinski, G. A. Baker, M. E. Tuckerman, R. F. Savinell, J. R. Sangoro, *Chem. Rev.* **2021**, *121*, 1232–1285.

[24] X. Meng, K. Ballerat-Busserolles, P. Husson, J. M. Andanson, *New J. Chem.* **2016**, *40*, 4492–4499.

[25] D. De Sloovere, D. E. P. Vanpoucke, A. Paulus, B. Joos, L. Calvi, T. Vranken, G. Reekmans, P. Adriaensens, N. Eshraghi, A. Mahmoud, F. Boschini, M. Safari, M. K. Van Bael, A. Hardy, *Adv. Energy Sustain. Res.* **2022**, *3*, 2100159.

[26] O. E. Geiculescu, D. D. Desmarteau, S. E. Creager, O. Haik, D. Hirshberg, Y. Shilina, E. Zinigrad, M. D. Levi, D. Aurbach, I. C. Halalay, *J. Power Sources* **2016**, *307*, 519–525.

[27] A. Boisset, J. Jacquemin, M. Anouti, *Electrochim. Acta* **2013**, *102*, 120–126.

[28] R. S. Kühnel, S. Obeidi, M. Lübke, A. Lex-Balducci, A. Balducci, *J. Appl. Electrochem.* **2013**, *43*, 697–704.

[29] M. S. Wu, T. L. Liao, Y. Y. Wang, C. C. Wan, *J. Appl. Electrochem.* **2004**, *34*, 797–805.

[30] J. Wang, Y. Yamada, K. Sodeyama, C. H. Chiang, Y. Tateyama, A. Yamada, *Nat. Commun.* **2016**, *7*, 1–9.

[31] K. Yoshida, M. Nakamura, Y. Kazue, N. Tachikawa, S. Tsuzuki, S. Seki, K. Dokko, M. Watanabe, *J. Am. Chem. Soc.* **2011**, *133*, 13121–13129.

[32] O. S. Hammond, D. T. Bowron, K. J. Edler, *Green Chem.* **2016**, *18*, 2736–2744.

[33] K. A. Hansen, J. Nerkar, K. Thomas, S. E. Bottle, A. P. O'Mullane, P. C. Talbot, J. P. Blinco, *ACS Appl. Mater. Interfaces* **2018**, *10*, 7982–7988.

[34] P. Azaïs, L. Duclaux, P. Florian, D. Massiot, M.-A. Lillo-Rodenas, A. Linares-Solano, J.-P. Peres, C. Jehoulet, F. Béguin, *J. Power Sources* **2007**, *171*, 1046–1053.

[35] K. Nakahara, J. Iriyama, S. Iwasa, M. Suguro, M. Satoh, E. J. Cairns, *J. Power Sources* **2007**, *165*, 398–402.

[36] J. K. Kim, J. H. Ahn, G. Cheruvally, G. S. Chauhan, J. W. Choi, D. S. Kim, H. J. Ahn, S. H. Lee, C. E. Song, *Met. Mater. Int.* **2009**, *15*, 77–82.

[37] A. Tornheim, D. C. O'Hanlon, *J. Electrochem. Soc.* **2020**, *167*, 110520.

[38] Y. Dai, Y. Zhang, L. Gao, G. Xu, J. Xie, *Electrochem. Solid-State Lett.* **2010**, *13*, 22–25.

Entry for the Table of Contents

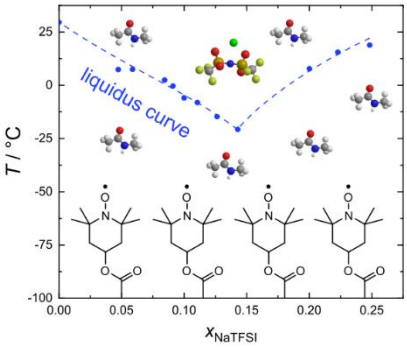

Sustainable battery technology:

The combination of deep eutectic solvents (DESs) with TEMPO-based electrodes opens a new way to environmentally friendly energy storage in all-organic batteries. Especially the eutectic mixture of the DES composed of sodium bis(trifluoromethanesulfonyl)imide and *N*-methylacetamide enables stable and efficient cycling of the polymer electrodes.

Supporting Information

Combining Deep Eutectic Solvents with TEMPO-based Polymer Electrodes: Influence of Molar Ratio on Electrode Performance

Matthias Uhl,[a] Tanja Geng,[a] Philipp A. Schuster,[b] Benjamin W. Schick,[a] Matthias Kruck,[a] Alexander Fuoss,[a] Alexander J. C. Kuehne[b] and Timo Jacob*[a.c.d]

[a] M. Uhl, T. Geng, B. W. Schick, M. Kruck, A. Fuoss, Prof. Dr. T. Jacob
Institute of Electrochemistry
Ulm University
Albert-Einstein-Allee 47, 89081 Ulm, Germany
E-mail: timo.jacob@uni-ulm.de

[b] P. Schuster, Prof. Dr. A. J. C. Kuehne
Institute of Organic and Macromolecular Chemistry
Ulm University
Albert-Einstein-Allee 11, 89081, Ulm, Germany

[c] Prof. Dr. T. Jacob
Helmholtz-Institute Ulm (HIU) for Electrochemical Energy Storage
Helmholtzstr. 11, 89081 Ulm, Germany

[d] Prof. Dr. T. Jacob
Karlsruhe Institute of Technology (KIT)
P.O. Box 3640, 76021 Karlsruhe, Germany

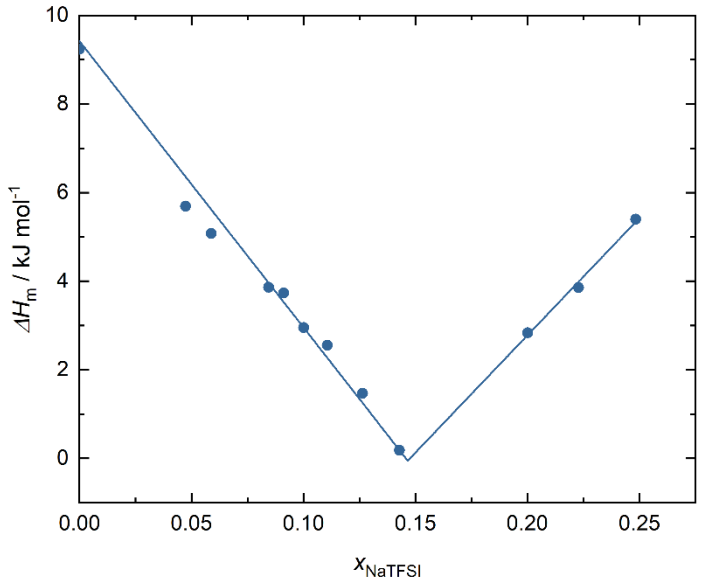

Figure S1. Enthalpy of the melting peaks determined from the DSC curves in Figure 1A, fitted by a two-part piecewise linear fit to determine the minimum.

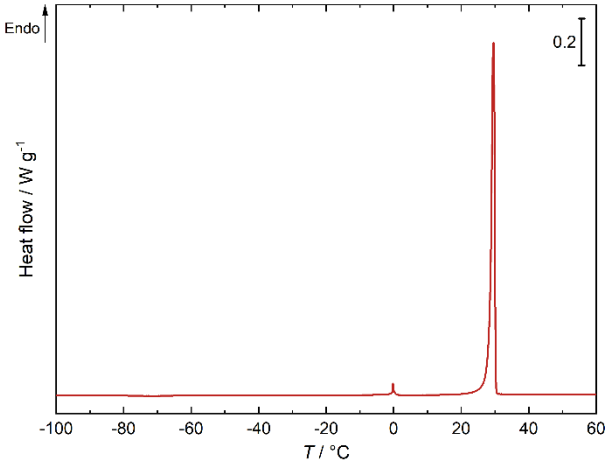

Figure S2. DSC curve of NMA recorded with a heating rate of 1 °C min^{-1} from -180 to 80 °C. The endothermic heat flow is shown as a function of temperature between -100 and 60 °C. The onset temperature of the melting is at 23.6 °C and the peak occurs at 29.6 °C. The purity of NMA determined from the DSC curve is approximately 99.5%.

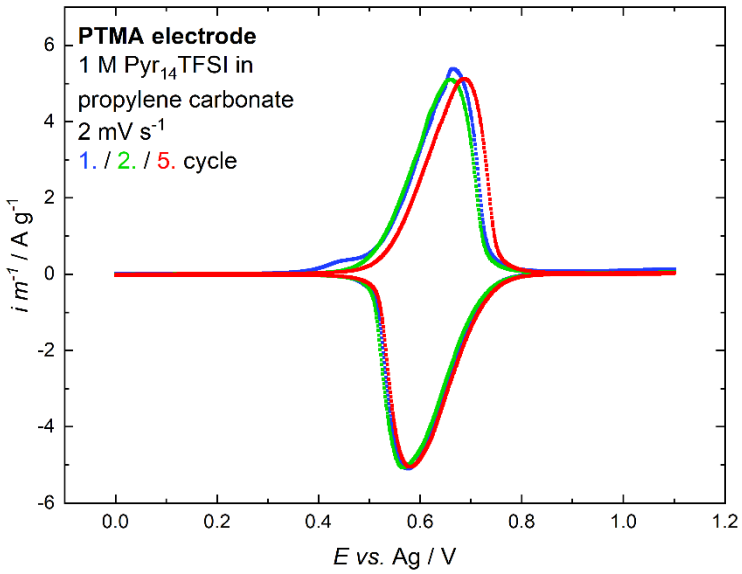

Figure S3. Cyclic voltammogram of a PTMA electrode in 1 M 1-butyl-1-methylpyrrolidinium bis(trifluormethylsulfonyl)imid ($Pyr_{14}TFSI$) in propylene carbonate showing the first (blue), second (green), and fifth (red) cycle at a scan rate of 2 $mV \cdot s^{-1}$.

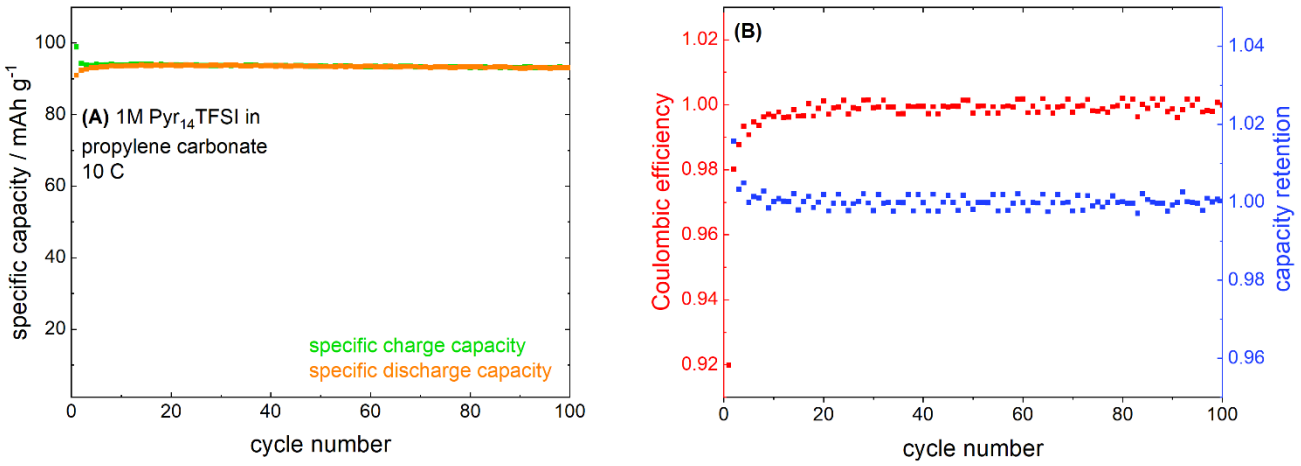

Figure S4. Chronopotentiometric charge-discharge cycling of a PTMA electrode in 1 M $Pyr_{14}TFSI$ in propylene carbonate between 0 V and 1 V *vs.* Ag at a rate of 10 C. (A) Specific charge (green) and discharge (orange) capacities for 100 cycles; (B) corresponding Coulombic efficiency (red) and capacity retention (blue).

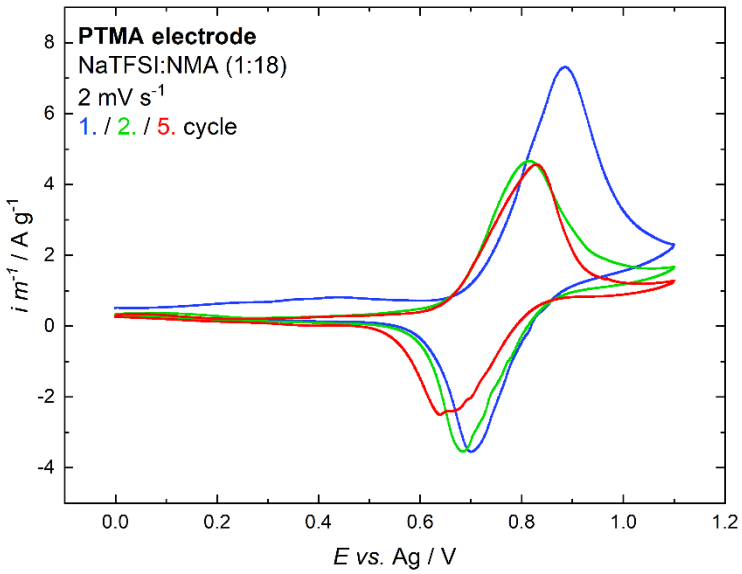

Figure S5. Cyclic voltammogram of a PTMA electrode in NaTFSI:NMA DES with a molar ratio of 1:18 showing the 1st (blue), 2nd (green), and 5th (red) cycle at a scan rate of 2 mV·s^{-1}.

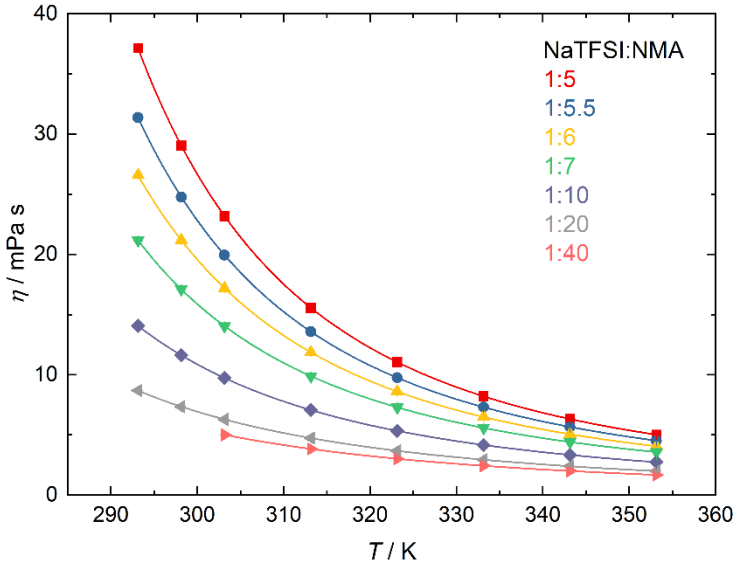

Figure S6. Dynamic viscosities of NaTFSI:NMA mixtures in different molar ratios as a function of temperature. The points are measured values and the lines correspond to exponential fits according to the VFT model.

For evaluation of the temperature dependence of the viscosity, a plot of the dynamic viscosity as a function of temperature is used (Figure S6). The curves exhibit an exponential decay and follow the Vogel-Fulcher-Tamman (VFT) model (Equation S1)[1], which describes liquids over a wide temperature range, including close to their melting points and in the supercooled region.[2,3]

$$\eta = \exp\left(A + \frac{B}{T - T_0}\right) \tag{S1}$$

Hereby, A, B, and T_0 are constants. The model is valid for non-spherical molecules or ions if molecular rotation is restricted and is often used for rather viscous, glass-forming liquids to include contributions of intermolecular interactions such as hydrogen bonding.[4] So far, the VFT model has been applied to various ionic liquids as well as DESs, which were mostly choline-based DESs type III.[5–8] For DESs type IV, for example, the viscosity of a LiTFSI:NMA 1:4 mixture (x_{LiTFSI} = 0.2) was analyzed, which also exhibits a temperature dependence according to the VFT model.[9]

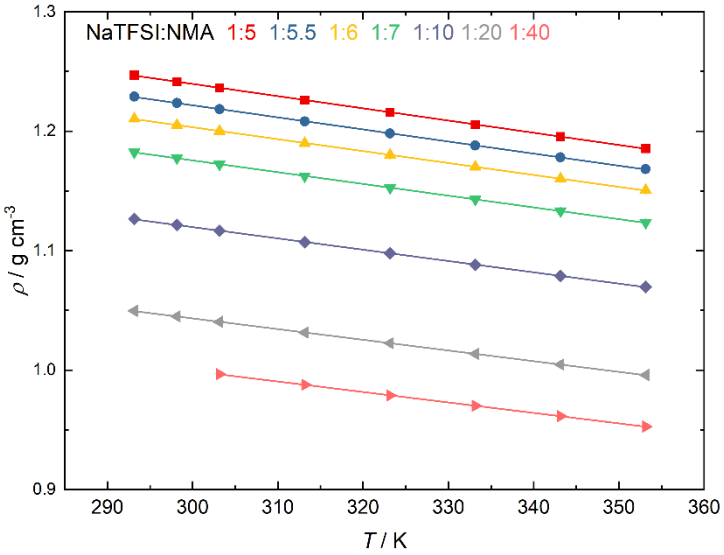

Figure S7. Densities of NaTFSI:NMA mixtures in different molar ratios as a function of temperature. The points are measured values and the lines correspond to linear fits.

The density ρ increases with increasing NaTFSI content and decreases with temperature (Figure S7). The temperature dependence is linear and follows Equation S2 with the constants ρ_0 and a, which depend on the molar ratio of the DES. The same linear behavior is known for other DESs.[10,11] The values themselves at 20 °C (1.246 g·cm^{-3} for NaTFSI:NMA 1:5, 1.126 g·cm^{-3} for 1:10) are similar to the ones of NaTFSI:NMA mixtures previously reported (1.262 g·cm^{-3} for 1:4, 1.167 g·cm^{-3} for 1:9).[12]

$$\rho = \rho_0 + aT \qquad \text{(S2)}$$

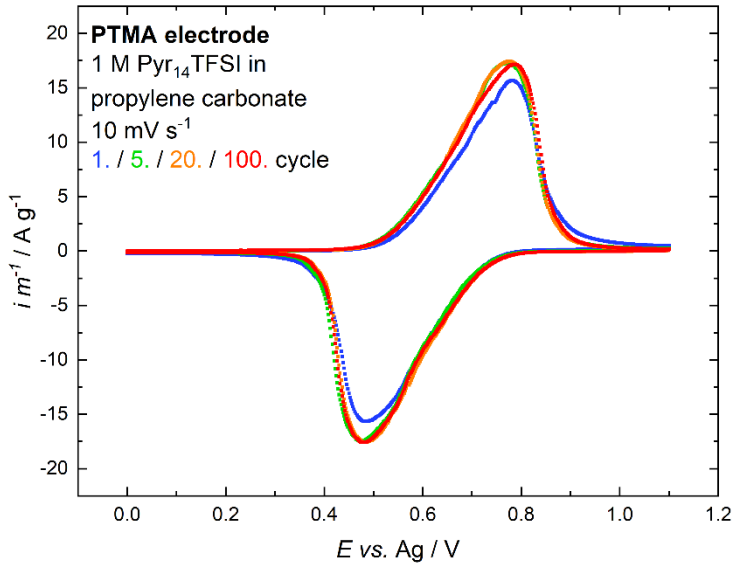

Figure S8. Cyclic voltammogram of a PTMA electrode in 1 M $Pyr_{14}TFSI$ in propylene carbonate for testing the cycling stability at a scan rate of 10 mV·s^{-1}. The 1st (blue), 5th (green), 20th (orange), and 100th (red) cycle are shown.

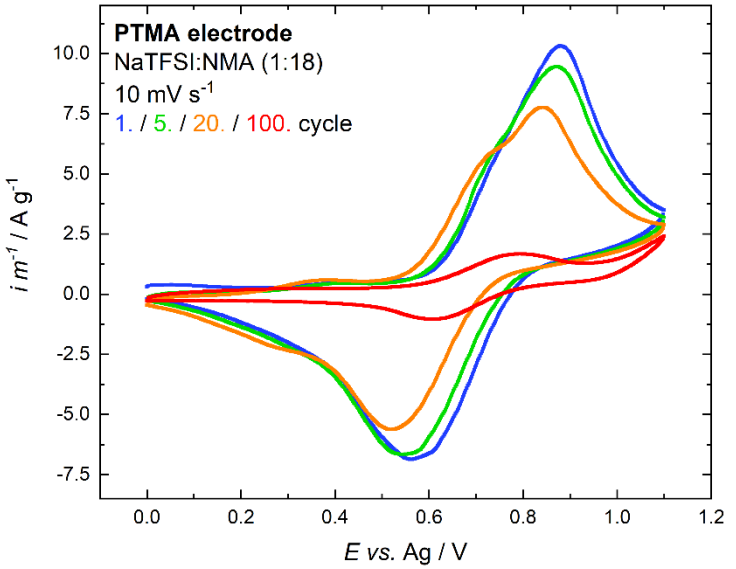

Figure S9. Cyclic voltammogram of a PTMA electrode in NaTFSI:NMA DES with a molar ratio of 1:18 for testing the cycling stability at a scan rate of 10 mV·s^{-1}. The 1st (blue), 5th (green), 20th (orange), and 100th (red) cycle are shown.

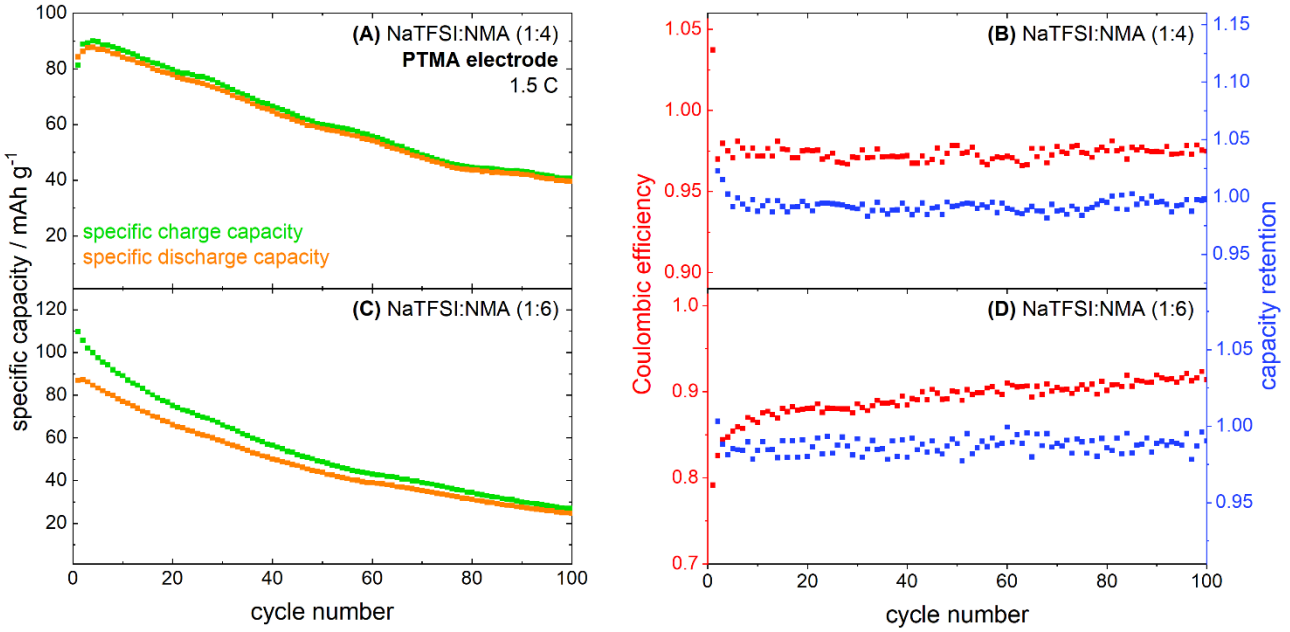

Figure S10. Chronopotentiometric charge-discharge cycling of PTMA electrodes in NaTFSI:NMA DESs with a molar ratio of (A,B) 1:4 and (C,D) 1:6 between 0 V and 1 V *vs*. Ag at a rate of 1.5 C. (A,C) Specific charge (green) and discharge (orange) capacities for 100 cycles; (B,D) corresponding Coulombic efficiency (red) and capacity retention (blue).

References

[1] G. S. Fulcher, *J. Am. Ceram. Soc.* **1925**, *8*, 339–355.

[2] D. B. Davies, A. J. Matheson, *Trans. Faraday Soc.* **1967**, *63*, 596.

[3] H. Jin, B. O'Hare, J. Dong, S. Arzhantsev, G. A. Baker, J. F. Wishart, A. J. Benesi, M. Maroncelli, *J. Phys. Chem. B* **2008**, *112*, 81–92.

[4] J. F. Mano, E. Pereira, *J. Phys. Chem. A* **2004**, *108*, 10824–10833.

[5] B. B. Hansen, S. Spittle, B. Chen, D. Poe, Y. Zhang, J. M. Klein, A. Horton, L. Adhikari, T. Zelovich, B. W. Doherty, B. Gurkan, E. J. Maginn, A. Ragauskas, M. Dadmun, T. A. Zawodzinski, G. A. Baker, M. E. Tuckerman, R. F. Savinell, J. R. Sangoro, *Chem. Rev.* **2021**, *121*, 1232–1285.

[6] A. Yadav, S. Pandey, *J. Chem. Eng. Data* **2014**, *59*, 2221–2229.

[7] F. S. Mjalli, J. Naser, *Asia-Pacific J. Chem. Eng.* **2015**, *10*, 273–281.

[8] A. Bakhtyari, R. Haghbakhsh, A. R. C. Duarte, S. Raeissi, *Fluid Phase Equilib.* **2020**, *521*, 112662.

[9] A. Boisset, J. Jacquemin, M. Anouti, *Electrochim. Acta* **2013**, *102*, 120–126.

[10] A. Hayyan, F. S. Mjalli, I. M. Alnashef, T. Al-Wahaibi, Y. M. Al-Wahaibi, M. A. Hashim, *Thermochim. Acta* **2012**, *541*, 70–75.

[11] R. K. Ibrahim, M. Hayyan, M. A. AlSaadi, S. Ibrahim, A. Hayyan, M. A. Hashim, *J. Mol. Liq.* **2019**, *276*, 794–800.

[12] D. De Sloovere, D. E. P. Vanpoucke, A. Paulus, B. Joos, L. Calvi, T. Vranken, G. Reekmans, P. Adriaensens, N. Eshraghi, A. Mahmoud, F. Boschini, M. Safari, M. K. Van Bael, A. Hardy, *Adv. Energy Sustain. Res.* **2022**, *3*, 2100159.